The Evaporative Demand Drought Index: Part II – CONUS-wide Assessment Against Common Drought Indicators

Daniel McEvoy[1], Justin Huntington[1], Michael Hobbins[2,3], Andrew Wood[4], and Charles Morton[1]

[1]Desert Research Institute, Reno, NV

[2]University of Colorado-Cooperative Institute for Research in Environmental Sciences, Boulder, CO

[3]NOAA-Earth Systems Research Laboratory, Physical Sciences Division, Boulder, CO

[4]National Center for Atmospheric Research, Boulder, CO

Abstract

Precipitation, soil moisture, and air temperature are the most commonly used climate variables to monitor drought, however other climatic factors such as solar radiation, wind speed, and specific humidity can be important drivers in the depletion of soil moisture and evolution and persistence of drought. This work provides an assessment of the Evaporative Demand Drought Index (EDDI) at multiple time scales for several hydroclimates as a companion study to Hobbins et al. (2015) by examining EDDI and individual evaporative demand components as they relate to the dynamic evolution of flash drought over the central US, characterization of hydrologic drought over the western US, and comparison to commonly used drought metrics of the US Drought Monitor, Standardized Precipitation Index (SPI), Standardized Soil Moisture Index (SSI), and the Evaporative Stress Index (ESI). Results show that EDDI has the strongest relationships to SPI and SSI over Texas, Oklahoma, and much of the desert Southwest, while comparisons to summer ESI revealed a hotspot over much of the central US. At short time scales, spatial distributions and time series results illustrate that EDDI is useful for flash drought identification, and can serve as a leading indicator by as much as two months in advance of the USDM, SPI, and SSI. Our results illustrate the benefits of physically based evaporative demand estimates, and demonstrate EDDI's utility and effectiveness in an easy-to-implement operational early warning and long-term hydrologic drought monitoring tool for agricultural and drought monitoring, and potential application to seasonal forecasting and fire-weather monitoring.

1. Introduction

Drought is a complex and naturally occurring process with adverse effects on society, primarily through degradation and loss of agricultural crops and depletion of water resources (i.e., streamflow and reservoir storage). Recent examples are instructive: in California, the extended drought that began in late 2011 is still ongoing, and the 2011-2014 three-year average precipitation (Prcp) record indicates that this period is the second driest in recorded history (Seager et al., 2015); in 2011, Texas experienced extreme Prcp deficits; while in 2011 and 2012 record-breaking temperatures (T_{air}) and high wind speed (U_z) played a significant role in drought intensification over much of the central US (Karl et al. 2012, Cattiaux and Yiou 2013). Total economic losses are estimated to be $2.7 billion, $7.7 billion, and more than $35 billion for the California, Texas, and central US droughts, respectively. While conditions in Texas deteriorated over many months in 2011, the depletion of moisture over the central US in 2011 occurred at a much faster rate. This fast onset of drought has recently been termed "flash drought" (Svoboda et al. 2002). The physical mechanisms driving flash droughts have been largely neglected from traditional drought metrics. Hence there is a growing need for continued development of physically based drought metrics that capture important land surface-atmospheric feedbacks, and provide sufficient early warning.

It has been common practice in recent decades to monitor and analyze drought using metrics driven by Prcp and T_{air} only. The two most commonly used drought indices are the Palmer Drought Severity Index [PDSI; Palmer (1965)], which relies on monthly T_{air} and Prcp, and the Standardized Precipitation Index [SPI; McKee (1993)], which relies on Prcp only. While the PDSI and SPI have proven useful for providing valuable information regarding hydrologic and meteorological drought, these metrics have limitations at short time scales and fail to account for the effects of other important drought meteorological and radiative forcings such as specific humidity (q), U_z, and downwelling shortwave radiation (R_d). The most heavily used dataset for decision making with regards to drought is the US Drought Monitor [USDM; Svoboda et al.

(2002)], which relies on a blend of metrics (including PDSI and SPI) and climate data (e.g., soil moisture (SM), streamflow, and snow water equivalent) to produce weekly maps of drought severity. The USDM could be improved through the inclusion of important hydrometeorological forcings key to identifying flash and long-term drought through the use of physically based evaporative demand (E_0) estimates.

Other operational products could similarly be improved with the inclusion of physically based E_0 estimates. For example, the U.S. operational PDSI, produced by the National Oceanic and Atmospheric Administration (Heddinghaus and Sabol 1991), continues to use T_{air}-based E_0 estimates (i.e. Thornthwaite 1948) within the PDSI formulation despite the fact that there have been a number of studies that recommend the use of physically based formulations of E_0 (Milly and Dunne 2011; Hobbins et al. 2008, 2012; Hobbins 2015). Both Dai (2011) and van der Schrier et al. (2011) found PDSI to be largely insensitive to E_0 parameterization during the 20th and early 21st century. On the other hand, Sheffield et al. (2012) found major differences between the PDSI driven with T_{air}- and physically-based E_0 estimates, especially from the mid-1990s through 2008, with T_{air}-based E_0 estimates showing a significant drying trend in PDSI, and physically based E_0 estimates indicating no significant trend in global drought severity. The role of physically based E_0 estimates in drought monitoring and prediction remains an active—and to some degree, controversial—area of research, and is a focus of this paper.

Recent studies have shown that actual evapotranspiration (ET), which is obtained through the use of thermal and optical satellite remote sensing or land surface models, used in combination with physically based E_0 can be used as a drought indicator by inherently accounting for feedbacks between the land surface-atmosphere interface through the use of ratios of ET to E_0 (Yao et al. 2010; Anderson et al. 2007a, 2007b, 2011; Mu et al. 2013; Otkin et al. 2013a, 2013b).

However, the use of thermal and optical remote sensing data for operational drought monitoring has limitations, such as cloud cover, spurious ET estimates in semi-arid and arid regions, satellite inter-arrival times that have to be interpolated, and uncertain simulated surface energy balance in mountainous regions, especially where seasonal snowpack exists.

In an effort to complement and overcome some of the limitations of the aforementioned metrics, the companion paper (Hobbins et al. – this issue) developed the Evaporative Demand Drought Index (EDDI), which relies solely on physically based E_0 estimates derived from a near-real-time (2-5 day latency), easily accessible land surface forcing dataset: the North American Land Data Assimilation System Phase-2 [NLDAS-2; Mitchell et al. (2004)]. Hobbins et al. (this issue) describe two primary physical feedbacks between ET and E_0 that form the rationale for EDDI: a complementary relationship under water-limited conditions (extended drought) where ET and E_0 vary in opposing directions (Bouchet 1963), and parallel variations under energy-limited conditions at the onset of flash drought. Under both scenarios, EDDI was found to respond to drying and wetting anomalies of major components of the hydrologic cycle at various time scales (Hobbins et al. - this issue).

This paper builds upon the work of Hobbins et al. (this issue) through a robust CONUS-wide assessment of EDDI against several commonly used drought indices, and outlines a second standardization option that acts to reduce errors in comparing multiple drought indices through space and time. Data sources, E_0 formulation, and statistical procedures to calculate EDDI are presented first, followed by comparisons of EDDI to other commonly used drought metrics, a flash drought case study over the central US, and finally, extended drought case studies over the western US.

2. Data and Methods

2.1. Evaporative demand

Daily bias-corrected and spatially disaggregated (from 12 km to 4 km) NLDAS-2 gridded meteorological data [METDATA; Abatzoglou (2011)] are used to compute E_0 on a daily basis for 1979 to 2013. Maximum and minimum temperature at 2-m (T_{max} and T_{min}), *q* at 2-m, R_d, and 10-m wind speed (U_{10}) were obtained from the University of Idaho (http://metdata.northwestknowledge.net/). A variety of methods has been developed to compute E_0 including T_{air}-based methods (e.g., Thornthwaite 1948, Hargreaves and Samani 1985), radiation-based methods (Priestley and Taylor 1972), and radiation - aerodynamic combination methods that incorporate T_{max}, T_{min}, R_d, U_{10}, and *q*, such as the Penman-Monteith (PM) approach (Monteith 1965). A priori, it is generally assumed that if the necessary data resources are available, a full-form physically based method, such as PM, should be used over methods based only on T_{air} or radiation. Hobbins et al. (2012) and Hobbins (2015) demonstrated that the primary drivers of E_0 variability differ across the US, and with aggregation period (e.g., monthly vs. annual) and season. For example, during summer months U_{10} is the primary driver of E_0 variability over much of the Great Basin, while R_d is the primary driver of variability over much of the southeast US. In this study, we use reference ET (ET_0) from the PM-based American Society of Civil Engineers Standardized Reference ET equation (ASCE-EWRI, 2005) for E_0.

2.2 Evaporative Demand Drought Index

A probability-based standardized climate variable can be obtained using parametric or non-parametric methods. Parametric methods use a single probability distribution to fit a time series (e.g., Gamma distribution for SPI), where probabilities are transformed to standardized values through an inverse normal approximation. However, a single probability distribution may not always be appropriate at large spatial scales, and several studies have documented these limitations with SPI (Guttman 1999; Quiring 2009) and Standardized Streamflow Index (Vicente-Serrano et al. 2012). The Evaporative Demand Drought Index (EDDI) presented in Hobbins et al. (this issue) is calculated from a simple Z-score based on the mean and standard deviation of a given accumulated ET_0 time series. Here, we deviate from Hobbins et al. (this issue) by using a probability-based approach for EDDI to allow for more consistent comparisons between EDDI against other standardized indices.

To overcome the limitations of a parametric approach, ET_0 probabilities (*P(x)*) are obtained through the empirical Tukey plotting position (Wilkes 2011):

$$P(x_i) = \frac{i - 0.33}{n + 0.33},$$

where i is the rank in the historical time series (from 1 to 35, with 1 being the max ET_0 value and 35 being the min) of the observed value, and n is the number of observations. EDDI values are obtained from empirically derived probabilities through an inverse normal approximation (Abramowitz and Stegun 1965) at time scales of 1, 3, 6, 9, and 12 months. Comparisons between EDDI values derived from the simple z-score outlined in Hobbins et al. (this issue) and the formulation presented here showed negligible differences in identifying wet and dry periods, but the plotting position approach was ultimately chosen in this paper to maintain consistency when comparing multiple indices outlined below. This method follows Hao and AghaKouchak (2014), where the plotting position approach was used to compute SPI, Standardized Soil Moisture Index (SSI) and Multivariate Standardized Drought Index (MSDI). Farahmand and AghaKouchak (2015) recommend this plotting position approach to maintain consistency when comparing several standardized drought indices.

2.3 NLDAS-based drought metrics

To assess the ability of EDDI to identify historical drought periods, EDDI is compared to SPI and SSI using monthly Prcp and simulated SM from NLDAS-2 (Xia et al. 2012a, 2012b). NLDAS-2 Prcp is primarily derived from Climate Prediction Center gridded daily gauge data {with a topographical adjustment from the Parameter-elevation Regressions on Independent Slopes Model [PRISM; Daly et al. (1994)]}. NLDAS-2 SM is derived from the Variable Infiltration Capacity land surface model [VIC; Liang et al. (1994)], and represents the average SM from the top 100 cm of the soil column. Monthly NLDAS-2 data were obtained for the period of 1979 to 2013 with a native grid spacing of 0.125°. To compare EDDI to NLDAS-2 drought indices, all NLDAS-2 data were resampled to the 4-km (~1/16°) UI METDATA grid using a bilinear interpolation. Monthly Prcp and SM were accumulated at five time scales (1, 3, 6, 9, and 12 months), and standardized following the EDDI methodology of plotting positions and inverse normal approximation. Pearson linear correlation coefficients between EDDI and standardized NLDAS-2 variables were computed for each month ($n = 35$ years) at the five time scales.

2.4 Evaporative Stress Index

The ESI (Anderson et al. 2007b, 2011) represents standardized anomalies in the ET fraction of reference ET (i.e., ET/ET_0), with ET obtained through satellite-assisted modeling of the land surface energy balance. ET and other land-surface energy balance components are retrieved using satellite optical and thermal imagery, to force the Atmosphere-Land Exchange Inverse surface energy balance model [ALEXI; Anderson et al. (1997, 2007a)]. Atmospheric variables needed to drive ALEXI come from the North American Regional Reanalysis [NARR; Mesinger et al. (2006)].

Weekly ESI data were provided (courtesy of Martha Anderson, USDA, and Chris Hain, University of Maryland) over the US for 2000 to 2013 at a 4-km spatial resolution and were aggregated to time scales of 1, 2, and 3 months. To obtain a constant comparison between EDDI and ESI, EDDI was recalculated using the same period of record as the ESI, and the same aggregation time scales. ESI data were resampled using a bilinear interpolation to match the EDDI grid. No downscaling was necessary as both grids were of identical spatial resolution. Pearson linear correlation coefficients between EDDI and ESI were computed for each week over the 14-year period and at all five time scales.

2.5 United States Drought Monitor

The USDM (Svoboda et al. 2002) was used as another metric to validate EDDI, with the primary goal of identifying differences between the two metrics during the evolution of drought through time and space. The USDM is derived from a blend of drought metrics adjusted using local expert knowledge to develop weekly drought severity maps over CONUS (Svoboda et al. 2002; Anderson et al. 2013). The USDM classification system of drought ranges from D0 (abnormally dry) to D4 (exceptional drought). For results where the USDM is compared, all drought metrics were converted to USDM classes (Table 1). The comparisons of EDDI to the USDM are necessarily qualitative because the USDM is a blend of information at several different time scales, whereas EDDI represents a single time scale.

< Table 1 here >

USDM data (2000 to 2013) were downloaded as ESRI shapefiles provided by the National Drought Mitigation Center, and rasterized to match the 4-km EDDI grid, to create a USDM class map of integer values of drought intensity ranging from 0 to 4 (i.e., D0 = 0, D1 = 1, D2 = 2, D3 = 3, and D4 = 4);

3. Results and Discussion

3.1 NLDAS-2 drought index correlations with EDDI

Correlations between EDDI and NLDAS-2 drought indices (EDDI-SPI and EDDI-SSI) for 1, 6, and 12 month time scales are shown in Figure 1. Positive EDDI values indicate drought, and negative SPI and SSI values indicate drought, therefore strong negative correlations represent similar drought signals between EDDI and both SPI and SSI over the 35-year period of record. At the 1-to 12-month time scales correlations between EDDI and SPI and SSI are strongest (more negative) over much of the southwestern and southcentral US (with the exception of 1-month SSI), and highest in Texas (r <-0.7). The northeast is region of general weak correlations for both EDDI-SPI and EDDI-SSI, with the Midwestern states of OH, IN, and MI being a weak spot for EDDI-SPI only. Spatial correlations at 6 and 12 month time scales are quite similar (Figure 1c-1f), and generally much stronger than at the 1-month time scale (Figure 1a and 1b). Over the northeastern US, EDDI-SPI correlations remain fairly weak at longer timescales, while EDDI-SSI correlations improve over OH, WV, NY, and PA (Figure 1c-1f).

Weak correlations to 1-month SSI over the west may be explained by above average T_{air} and R_d (driving EDDI upwards) that can lead to increased snow melt and SM, and a short term wetting signal from SSI, particularly during the winter months. Positive correlations of EDDI-SPI and EDDI-SSI over the northeastern US are caused by energy-limited conditions as opposed to water-limited conditions. In such energy-limited regions, the rate of change in ET is generally proportional and in the same direction as ET_0 (Han et al. 2014; Hobbins et al. - this issue).

< Figure 1 here >

Figure 2 highlights four regions of interest selected for individual monthly correlation analysis. The Central Valley of California (CA) and Iowa (IA) are two major agricultural regions where drought impacts can have adverse effects on crop production. East-central Texas (TX) is part of a region that has been identified as a global “hot spot” for strong land surface-atmospheric coupling (Koster et al. 2004, 2006); therefore strong correlation of SM and Prcp to EDDI is expected. Pennsylvania (PA) is an area identified by Koster et al. (2009) where SM is generally high and exerts little control on ET due to prevailing energy limiting conditions, even during times of severe meteorological drought. This observation is consistent with low correlations found in Figure 1 in parts of the northeast US. The following section further highlights how ET_0 anomalies (i.e., EDDI) in PA relate to SM- and Prcp-driven droughts.

< Figure 2 here >

Individual monthly correlations between EDDI and NLDAS-2 derived indices at various time scales are shown in Figure 3 for these regions of interest. For each of the selected regions shown in Figure 2, EDDI correlations to SSI and SPI were area-averaged over all pixels. For the TX region (Figure 3a and 3e), seasonality and time scale had little impact on the strength of correlations, and generally showed strong inverse relationships ($r < -0.6$ for SPI and $r < -0.7$ for SSI) during most months and time scales, reinforcing the conclusions of Koster et al. (2004, 2006).

For the CA region, large seasonal and time scale dependent variations were found, especially at the 1-month time scale for both SPI and SSI (Figure 3b and 3f). Correlations ranged from +0.20 to -0.82, with the highest correlations occurring at the 6- to 12-month time scales during the growing season. An exceptionally weak correlation (-0.13) was found with SPI during July at the 1-month time scale. July is the driest month of the year for the Central Valley of CA, and most Julys see zero Prcp accumulation. This limits the negative range of the 1-month SPI (McEvoy et al. 2012) causing poor correlations with EDDI. Furthermore, when it does rain during dry summer months it occurs from isolated convective activity over a single day: even if most of the month was warm, cloud-free, and dry (leading to a drought signal from EDDI), the SPI will show a wet anomaly. A more consistent stepped correlation pattern was revealed at longer time scales, where *r* values < -0.7 were found during the spring (April, May, and June) for 3-month, spring and summer (July, August, and September) for 6-month, and summer and fall (October, November, and December) for 9- and 12-month periods.

Iowa was similar to Texas in that little variability was found in correlations (*r*-values only ranged from -0.5 to -0.7), with the exception of the 1-month time scale. Lower correlations at 1-month time scale during the fall and winter should be expected with SSI, since the top 100 cm of ground is typically frozen during these months, and land surface-atmospheric coupling is weak. There is a rapid increase in correlation at the 1-month time scale during the late spring and summer.

Correlations for PA region were the weakest of the four analyzed, with notably higher correlation to SSI (Figure 3h) when compared to SPI (Figure 3d). For SPI (Figure 3d), *r*-values never exceed -0.56, while for SSI (Figure 3h) *r*-values ranged from -0.60 to -0.69 during the summer and early fall at 1-, 3- and 6-month time scales. Weak correlations were found to be both slightly positive and negative ($-0.30 < r < +0.20$) for SPI and SSI at the 1-month time scale during fall and winter, and for winter and spring months at other time scales. Results shown in Figure 3 illustrate that EDDI may be particularly useful for flash drought and seasonal drought monitoring, especially during the growing season.

< Figure 3 here >

Soil moisture is typically a slowly varying component of the hydro-climatic system compared to variations in ET_0; therefore EDDI could serve as a leading indicator for identifying soil moisture deficits. Correlations between EDDI and SSI at coincident time scale and ending month (as presented in Figure 3) may not be the most robust due to this time lag between SM and ET_0. To demonstrate the potential value of EDDI as a leading drought indicator during the growing season a lagged correlation analysis was performed between 3-month SSI ending in August and EDDI at every time scale and ending month.

Figure 4 shows that in all four regions EDDI leads SSI, where 3-month SSI ending in August (blue dots in Figure 4 show fixed time scale and ending month for SSI) is better correlated to 3-month EDDI ending in June (CA; Figure 4a) or July (TX, IA, and PA; Figure 4b, 4c, and 4d respectively). An interesting feature of Figure 4 is shown for IA, where 12-month EDDI ending in August was found to have highest correlation to 3-month SSI ending in August, highlighting the extremely low summer SM moisture variability in this region. This is further reinforced later in Figure 6, where monthly SSI variability was found to be low relative to EDDI and SPI during the 2012 drought. These results highlight that EDDI is a leading indicator when compared to SSI, and therefore could be used to complement and perhaps improve the USDM since SM percentiles are primary inputs for USDM objective blends.

< Figure 4 here >

3.2 ESI correlations with EDDI

Seasonal temporal correlations between EDDI and ESI for CONUS are shown in Figure 5. Only spring (April, May, and June) and summer (July, August, and September) periods are evaluated due to limited availability of continuous monthly ESI data during fall and winter. ESI data were frequently missing in snow-covered mountainous regions of the west during spring and summer periods, and ESI pixels were masked (indicated by white shading in Figure 5, as in the mountain ranges of western US) when less than 75% of the monthly time series was available over the period of 2000 to 2013. Pixels with spurious ESI data (ESI <-5 and >5) were also masked. One benefit of EDDI over ESI and other remote sensing based metrics is that EDDI can be used during all seasons. This may be particularly useful for high-elevation hydrometeorological monitoring in seasonally snow-covered areas.

Figure 5 illustrates fairly large differences between spring and summer periods, with negligible differences between different time scales of 4-, 8-, and 12-weeks. During the spring period negative correlations are strongest (r values < -0.7) over much of TX, the desert SW, and central valley of CA, while weaker relationships were found over the NE, and parts of the Pacific NW (Figure 5a, 5c, and 5e). The low positive correlations in the NE are due to energy-limited evaporative conditions described in section 3.1. Summer correlations (Figure 5b, 5d, and 5f) are strongest and spatial patterns most consistent over the central US, and lower correlations are evident over parts of NV, CA and into the Pacific Northwest when compared to the spring period. Inspection of the summer time series from the regions of low correlation in the west and Pacific Northwest showed that during certain summers ESI and EDDI were strongly negatively correlated, but positively correlated in others (not shown). ET rates in semi-arid regions are typically low during summer periods; therefore small variations in ET can potentially lead to large changes in ESI, making for poor correlations with EDDI. For example, most of NV experienced below normal Prcp and high temperatures for July of 2005, and EDDI and SPI indicated drought conditions, whereas ESI indicated wet conditions (not shown). In general, EDDI is strongly correlated to ESI (r values < -0.7) during spring and summer months over much of the southwest, southcentral, and northcentral US.

< Figure 5 here >

3.3 Flash drought over the central US

Flash drought can develop even during periods of excess Prcp, and evaporative drivers can potentially uniquely identify the onset and evolution of flash drought. For example, in some situations (i.e., the 2011 central CONUS case), a T-based E_0 would fail to identify rapid drying due to below normal T_{air} coincident with high U_2 and low q. The following highlights the Midwest droughts of 2011 and 2012 as a case study to demonstrate how EDDI can serve as an effective early warning of flash droughts, as well as extended droughts.

Area-averaged time series of 1-month EDDI are compared to 1-month SPI and SSI during 2011 and 2012 in Figure 6a for the IA domain. Figure 6b illustrates the sensitivity of EDDI to individual ET_0 forcings averaged over the IA domain. Note that in Figures 6a and 6b the vertical axis of EDDI is reversed to better visualize drought onset and duration when compared to SPI and SSI. Figure 6a illustrates that in April, 2011, all indices are near neutral (i.e., close to zero), and over the next two months EDDI changes to a moderate drought class (<-0.78 or USDM D1 class), while both SPI and SSI increase to slightly wet conditions. SPI and SSI values do not decrease towards moderate drought conditions until July of 2011. SPI falls below moderate drought in September, and SSI follows one month later in October. Both EDDI and SSI maintain extended drought conditions throughout all of 2012, with the exception of February when EDDI is slightly above moderate drought (-0.78), but still below zero. During this extended drought of 2012, SPI is highly variable and indicates wet conditions for many months.

To highlight the ET_0 drivers that caused EDDI to signal first a flash drought and then an extended drought, a simple sensitivity analysis of EDDI was performed (Figure 6b and 6c). For this analysis, ET_0 was calculated while constraining the variable of interest to daily climatology values in order to isolate the impact of each forcing on the EDDI drought signal. Results are presented as estimates of EDDI with a notation of the variable constrained to its daily climatology (i.e., EDDI-T, EDDI-q, EDDI-R_d, and EDDI-U_2). For example, EDDI-T was calculated using the daily climatology of T_{max} and T_{min}, and with METDATA-observed forcings values of all other variables. During the period of 20 May to 25 May, EDDI-q and EDDI-U_2 had the greatest separation from standard EDDI values in the negative direction (note y-axis is reversed), which indicates that the drying power of the air term in the ET_0 equation, (U_2 multiplied by vapor pressure deficit), initiated the flash drought signal—approximately 20 May through 5 June—in EDDI via increased U_2 and below normal *q* (Figure 6c). In this case, using daily climatology *q* and U_2 values mitigated the drought signal relative to the standard EDDI. By June, 2011, EDDI decreased below the moderate drought threshold (-0.78), with the primary difference from May being that U_2 and T_{air} were then acting in combination to exacerbate the drought signal—as opposed to T_{air} moderating it in May. Despite below-normal T_{air} conditions in September, 2011, the standard EDDI drought signal was maintained due to extremely low *q* values evidenced by a large difference between EDDI and EDDI-q (absolute difference of 1.17). From November, 2011, through the following May, T_{air} dominated the EDDI signal, as seen by the large differences between EDDI and EDDI-T. This increase in T_{air} and ET_0 likely contributed to the persistent SSI drought signal throughout 2012, despite above-normal Prcp for February, April, October, and December (Figure 6a).

Results illustrated in Figure 6 and in the companion paper of Hobbins et al. (2015) highlight two major focal points of this research: (1) EDDI is a leading indicator of flash and extended drought conditions, and (2) a physically based E_0 is required to capture this signal. This reinforces the work of Hobbins et al. (2012) and Hobbins (2015) who concluded that T_{air} is not always the dominant driver of ET_0, and T-based parameterizations could lead to false drying (or wetting) signals when used for drought monitoring applications. Our findings illustrated in

Figure 6 also contradict the notion that 2012 should be considered a flash drought case over the central US (e.g. Mo and Lettenmaier 2015): our results clearly indicate a well-established and persistent drought signal by both EDDI and SSI, with SPI being the only indicator to signal a rapid transition from wet to dry over the period of April through July. Figure 6 illustrates that the flash drought signal appeared in EDDI starting in May, 2011, and in SPI and SSI starting in August, 2011.

< Figure 6 here >

To spatially assess EDDI during the extended 2012 drought a comparison was made between the USDM, SPI, SSI, and ESI. Recall from Section 2.5 that the USDM is at a blended time-scale, against which a fixed time-scale EDDI is being compared: thus, the EDDI and the USDM distributions should not be expected to look similar. The objective of the EDDI and USDM comparisons is to show that EDDI can presage rapid onset droughts before the impacts show up in the USDM, thus highlighting the substantial added value gained by using EDDI in conjunction with other drought-monitoring metrics for decision-making applications.

Figure 7 shows the evolution of the 1-month EDDI, ESI, SSI, and SPI, and USDM through time and space over the spring and summer of 2012. The USDM generally indicated no drought or D1-D2 over much of the central US of 1 May. This is likely a result of the near-normal to slightly above normal Prcp during April, as illustrated in the April SPI spatial distribution. In contrast, EDDI indicates at least moderate drought conditions over most of the same region, and looks similar to the USDM spatial distribution two months later (i.e., of 3 July, 2012). EDDI responded to anomalously high T_{air}, U_2, and R_d across the region during the second half of April. ESI showed widespread neutral conditions for April with a rapid intensification in May. SSI and SPI show a slower progression and more local intensification (non-uniform spatial distribution) when compared to EDDI and ESI. The 2012 drought evolution illustrated by the USDM over the central US expands in both spatial extent and severity throughout the summer, however the progression from D0 to D3 and D4 takes approximately three months. Figure 7 illustrates that 1-month EDDI presaged the onset of USDM extreme to exceptional drought by as much as two months. ESI also led the onset of extreme to exceptional drought, but was limited in extent when respectively compared to April through July EDDI, and July USDM drought spatial distributions.

< Figure 7 here >

3.4 Extended drought in arid to semi-arid regions

In this section we examine whether EDDI can be used to characterize historical extended droughts over the western US. Droughts in arid to semi-arid regions of the US are generally slower to develop than in the central US, primarily due to the manner in which water resources are both naturally and anthropogenically stored. Natural water storage occurs as winter snowpack at high elevations that typically reach maximum depth in March or April. During spring and summer snowmelt, runoff is stored in reservoirs. Hydrologic and agricultural drought severity in the west are strongly linked to reservoir storage and streamflow (McEvoy et al. 2012, Abatzoglou et al. 2014).

Two extended drought case studies using the USDM, EDDI, SPI, and SSI are shown in Figure 8. The first case focuses on the drought of the 2007 water year (October 2006 through September 2007) (Figure 8, left column). The USDM from 02 October, 2007, indicates 78% (percent area) of the western US in at least a D0 drought class. Figure 8c illustrates the 12-month EDDI ending in September, 2007, and has the strongest spatial coherence and severity when compared to the USDM, while SSI and SPI (Figure 8e and 8g, respectively) underrepresent the spatial extent shown by USDM and EDDI, particularly over NV, ID, and western MT. The second case focuses on the extreme southwestern drought of 2002 (Figure 8, right column), with the USDM mapped at 25 June, 2002, and the 6-month EDDI, SPI, and SPI mapped for January through June, 2002. All metrics show a similar spatial structure of drought extent, although EDDI and SPI indicate little to no drought in MT. Temperatures were lower than normal over much of MT, WY, and the northern portion of UT and CO, and slightly above normal for the Four Corners region (not shown). This indicates that T_{air} was likely driving EDDI negative in MT, however T_{air}, q and U_2 must have all played a role in driving EDDI in the positive direction over UT and CO.

< Figure 8 here >

The potential usefulness of EDDI to aid in the interpretation of hydroclimatic states at multiple time scales and over long time periods was assessed for an area of interest. Figure 9 illustrates time series of EDDI averaged over the northern Sierra Nevada for 1979-2013. The northern Sierra Nevada provides much of the water resources to western NV and CA, therefore the use of multiple complementary drought metrics for evaluating short and extended drought in this region is invaluable. EDDI at the 2-wk and 1-month time scales (Figure 9a and 9b, respectively) closely correspond to documented heat waves and extreme fire weather in the region (Burt 2007; Trouet et al. 2009), however the high frequency of the time series make it difficult to characterize hydrologic drought. At longer time scales EDDI (Figure 9c, 9d, and 9e, respectively) clearly identify all of the major documented hydrologic droughts over the period from 1979 to 2013 (Seager 2007; Weiss et al. 2009; McEvoy et al. 2012). The longest duration drought to occur during the period of record analyzed was during the early 2000s, when the 12-month EDDI remained positive for five continuous years (late 1999 to 2005). Fast recovery of hydrologic droughts are also well captured by EDDI at nearly all time scales when compared to known "drought-buster" precipitation events (Ralph and Dettinger 2010; Dettinger 2013), and wet periods associated with El Niño (1982-83 and 1997-98), and La Niña (2010-11).

< Figure 9 here >

5. Summary and conclusions

This work highlights an application and assessment of EDDI at multiple time scales and for several hydroclimates as a companion study to Hobbins et al. (this issue). The methods and results of Hobbins et al. (this issue) are reinforced and a robust CONUS-wide evaluation is performed, by examining EDDI and individual evaporative demand components as they relate to the dynamic evolution of flash drought over the central US, characterization of hydrologic drought over the western US, and comparison to commonly used drought metrics (USDM, SPI, SSI, and ESI). Results highlight the advantages and limitations of EDDI as a monitor of drought at multiple time scales, and provide leading indications of flash and extended hydrologic drought. Correlations of EDDI to NLDAS-2 forced drought metrics of SSI and SPI indicate that over much of the CONUS, EDDI spatial distributions are generally similar to SPI and SSI. Over parts of the western US where weak correlations were found, EDDI often contained drought information not found in SPI or SSI. For example, Prcp is bounded by zero at short time scales (1 to 2 months) over many western states, which can lead to a skewed SPI, whereas EDDI will maintain a consistent distribution during months with no Prcp. At short time scales, spatial distributions and time series results illustrate that EDDI can be useful for flash drought identification, and can serve as a leading indicator by as much as two months in advance of the USDM, SPI, and SSI (i.e. Figures 4, 6, 7; and Figures shown in Hobbins et al. - this issue).

Comparisons of EDDI to remotely sensed ESI products also show strong correlations, with the exceptions of the northeast US during spring, and over parts of the western US during summer. Weak correlations with ESI over the northeastern US are largely due to energy-limited land-surface energy-balance conditions over the region, where ET and ET_0 are often positively correlated. Weak correlations with ESI over the western US during summer months are likely due to the low and effectively zero-bounded actual ET rates that occur in arid environments. Low soil moisture and low ET rates make it difficult to accurately estimate ET with thermal and optical remote sensing. These uncertainties combined with the high variability of estimated ET relative to average conditions often led to spurious ESI values and low correlations with EDDI. Comparisons of EDDI with ESI generally demonstrate that EDDI can be effectively used in conjunction with ESI and other remote sensing products to provide year-round data, with no limitations during cloudy days or over snow covered areas.

For drought monitoring in arid and semi-arid regions of western US, EDDI aggregation to longer time scales (3 to 12 months) is best suited to capture the complementary relationship found between ET and ET_0 (Bouchet 1963; Hobbins et al. 2004), and therefore identify extended hydrologic droughts typical of this region. Results illustrate that in most cases, when Prcp deficits at the 3- to 12-month time scales were fairly large, EDDI was strongly positive. However, the complementary relationship was found to not hold true in regions and time periods where weak land surface-atmospheric coupling and energy limited conditions exist (Figures 3 and 5).

Despite some noted limitations, EDDI is shown to provide useful information on the less-understood and documented dynamical processes associated with drought evolution and persistence. Results highlighted in this work illustrate the benefits of assimilating physically based E_0 estimates and EDDI into operational monitoring products such as the USDM. The additional information and early warning provided by EDDI could greatly contribute to a stronger understanding of drought evolution and dynamics, land surface-atmosphere interactions, and perhaps more importantly, reduce and/or mitigate future adverse societal effects that have been associated with past droughts. EDDI could also prove very useful and effective for easy-to-implement operational early warning for agricultural and fire-weather monitoring (Ham et al. 2014) and seasonal forecasting of drought.

Acknowledgments

This research was supported by the Desert Research Institute (DRI) Maki Endowment for enhancing water resource monitoring in Southern, Nevada, U.S. Bureau of Reclamation Climate Analysis Tools WaterSMART program, the National Integrated Drought Information System (NIDIS) program, and U.S. Geological Survey and DRI Great Basin Cooperative Ecosystem Study Unit collaborative project on drought monitoring and fallow field tracking through cloud computing of Landsat, MODIS, and gridded climate data archives.

References

Abatzoglou, J.T., 2011: Development of gridded surface meteorological data for ecological applications and modelling. *Int. J. Climatol*. **33**, 121–131, doi:10.1002/joc.3413.

Abatzoglou, J.T., R. Barbero, J. Wolf, and Z. Holden, 2014: Tracking interannual streamflow variability with drought indices in the U.S. Pacific Northwest. *J. Hydrometeor*. **15**, 1900–1912, doi:10.1175/JHM-D-13-0167.1.

Abramowitz, M., and I.A. Stegun, 1965: *Handbook of mathematical functions, with formulas, graphs, and mathematical tables*. Dover Publications, 1046 pp.

Anderson, M.C., J.M. Norman, G.R. Diak, W.P. Kustas, and J.R. Mecikalski, 1997: A two-source time-integrated model for estimating surface fluxes using thermal infrared remote sensing. *Remote Sens. Environ.*, **60**, 195–216.

Anderson, M.C., J. M. Norman, J.R. Mecikalski, J.A. Otkin, and W.P. Kustas, 2007: A climatological study of evapotranspiration and moisture stress across the continental United States based on thermal remote sensing: 1. Model formulation, *J. Geophys. Res.*, **112**, D10117, doi:10.1029/2006JD007506.

Anderson, M.C., J.M. Norman, J.R. Mecikalski, J.A. Otkin, and W.P. Kustas, 2007: A climatological study of evapotranspiration and moisture stress across the continental United States based on thermal remote sensing: 2. Surface moisture climatology, *J. Geophys. Res.*, **112**, D11112, doi:10.1029/2006JD007507.

Anderson, M.C., C. Hain, B. Wardlow, A. Pimstein, J.R. Mecikalski, and W.P. Kustas, 2011: Evaluation of drought indices based on thermal remote sensing of evapotranspiration over the continental United States. *J. Climate*, **24(8)**, 2025–2044, doi:10.1175/2010JCLI3812.1.

Anderson, M.C., C. Hain, J. Otkin, X. Zhan, K. Mo, M. Svoboda, B. Wardlow, and A. Pimstein, 2013: An intercomparison of drought indicators based on thermal remote sensing and NLDAS-2 simulations with U.S. Drought Monitor classifications. *J. Hydrometeor.*, **14**, 1035–1056, doi:10.1175/JHM-D-12-0140.1.

ASCE-EWRI, 2005: The ASCE Standardized Reference Evapotranspiration Equation. Report 0-7844-0805-X, 59 pp. [Available online at http://www.kimberly.uidaho.edu/water/asceewri/ascestzdetmain2005.pdf.]

Bouchet, R.J., 1963: Évapotranspiration réelle et potentielle, signification climatique. *Proc. International Association Scientific Hydrology Symp., Publ. No. 62*, Berkeley, CA, International Association Scientific Hydrology, 134–142.

Burt, C.C., 2007: *Extreme weather: a guide and record book*. W.W. Norton and Co., 320 pp.

Cattiaux, J., and P. Yiou, 2013: U.S. heat waves of spring and summer 2012 from the flow-analogue perspective [in “Explaining Extreme Events of 2012 from a Climate Perspective”]. *Bull. Amer. Meteor. Soc*., **94(9)**, S10–S13.

Dai, A., 2011: Characteristics and trends in various forms of the Palmer Drought Severity Index during 1900-2008, *J. Geophys. Res*., **116**, D12115, doi:10.1029/2010JD015541.

Daly, C., R.P. Neilson, and D.L. Phillips, 1994: A statistical-topographic model for mapping climatological precipitation over mountainous terrain. *J. Appl. Meteorol.*, **33(2)**, 140–158.

Dettinger, M.D., 2013. Atmospheric rivers as drought busters on the U.S. West Coast. *J. Hydrometeor.*, **14(6)**, 1721–1732, doi: 10.1175/JHM-D-13-02.1.

Farahmand, A., and A. AghaKouchak, 2015: A generalized framework for deriving nonparametric standardized indicators. *Adv. Water Resour.,* **76**, 140–145, doi:10.1016/j.advwatres.2014.11.012

Guttman, N.B., 1999: Accepting the standardized precipitation index: a calculation algorithm. *J. Amer. Water Resour. Assoc.* **35(2)**, 311–322.

Ham, C., M.T. Hobbins, K.L. Abt, and J.P. Prestemon, 2014: Using the Evaporative Demand Drought Index and the Palmer Drought Severity Index to forecast the number of large wildland fires on federal lands, *Large Wildland Fires Conference*, Missoula, MT, Association for Fire Ecology and the International Association of Wildland Fire. [Available online at http://largefireconference.org/wp-content/uploads/2013/06/Oral-Presentation-Abstracts-V4.pdf.]

Han, S., F. Tian, and H. Hu, 2014: Positive or negative correlation between actual and potential evaporation? Evaluating using a nonlinear complementary relationship model. *Water Resources Research*, 50(2), 1322–1336.

Hao, Z., and A. AghaKouchak, 2014: A nonparametric multivariate multi-index drought monitoring framework, *J. Hydrometeor.*, **15**, 89–101, doi:10.1175/JHM-D-12-0160.1.

Hargreaves, G.H., and Z.A. Samani, 1985: Reference crop evapotranspiration from temperature, *Appl. Eng. Agric*., **1**, 96–99.

Heddinghaus, T.R., and P. Sabol, 1991: A review of the Palmer Drought Severity Index and where do we go from here? *Preprints, Seventh Conf. on Applied Climatol*ogy, Boston, MA, Amer. Meteor. Soc., 242–246. [Available online at http://www.ncdc.noaa.gov/temp-and-precip/drought/docs/heddinghaus-sabol-pmdi-article.pdf.]

Hobbins, M.T., J.A. Ramírez, and T.C. Brown, 2004: Trends in pan evaporation and actual evaporation across the conterminous U.S.: Paradoxical or complementary? *Geophys. Res. Lett.*, **31(13)**, L13503, doi: 10.1029/2004GL0198426.

Hobbins, M.T., A. Dai, M.L. Roderick, and G.D. Farquhar, 2008: Revisiting the parameterization of potential evaporation as a driver of long-term water balance trends. *Geophys. Res. Lett.*, **35**, L12403, doi: 10.1029/2008GL033840.

Hobbins, M.T., A.W. Wood, D. Streubel, and K. Werner, 2012: What drives the variability of evaporative demand across the conterminous United States? *J. Hydrometeor.*, **13**, 1195–1214, doi: 10.1175/JHM-D-11-0101.1.

Hobbins, M.T., A. Wood, D.J. McEvoy, J.L. Huntington, C. Morton, and J. Verdin, 2015: The Evaporative Demand Drought Index: Part I - linking drought evolution to variations in evaporative demand. *J. Hydrometeor.* (this issue).

Hobbins, M.T., 2015: The variability of ASCE Standardized Reference Evapotranspiration: a rigorous, CONUS-wide decomposition and attribution. *Trans. ASABE* (accepted).

Karl T.R., and Coauthors, 2012: U.S. temperature and drought: recent anomalies and trends. *Eos Trans. AGU*, **93(47)**, 473–474.

Koster, R.D., and Coauthors, 2004: Regions of strong coupling between soil moisture and precipitation. *Science*, **305(5687)**, 1138–1140, doi: 10.1126/science.1100217.

Koster, R.D., and Coauthors, 2006: GLACE: The Global Land–Atmosphere Coupling Experiment. Part I: Overview. *J. Hydrometeor*., **7**, 590–610, doi:10.1175/JHM510.1.

Koster, R.D., S.D. Schubert, and M.J. Suarez, 2009: Analyzing the concurrence of meteorological droughts and warm periods, with implications for the determination of evaporative regime. *J. Climate*, **22**, 3331–3341, doi: 10.1175/2008JCLI2718.1.

Liang, X., D.P. Lettenmaier, E.F. Wood, and S.J. Burges, 1994: A simple hydrologically based model of land surface water and energy fluxes for general circulation models. *J. Geophys. Res.*, **99(D7)**, 14,415–14,428.

Mesinger, F., and Coauthors, 2006: North American Regional Reanalysis. *Bull. Amer. Meteor. Soc*., **87(3)**, 343–360, 10.1175/BAMS-87-3-343

McEvoy, D.J., J.L. Huntington, J.T. Abatzoglou, and L.M. Edwards, 2012: An evaluation of multiscalar drought indices in Nevada and eastern California. *Earth Interact*., **16**, 1–18, doi:10.1175/2012EI000447.1.

McKee, T.B., N.J. Doesken, and J. Kleist, 1993: The relationship of drought frequency and duration to time scales. *Preprints, Eighth Conf. on Applied Climatology*, Anaheim, CA, Amer. Meteor. Soc., 179–184. [Available online at http://ccc.atmos.colostate.edu/relationshipofdroughtfrequency.pdf.]

Milly, P.C.D., and K.A. Dunne, 2011: On the hydrologic adjustment of climate-model projections: the potential pitfall of potential evapotranspiration. *Earth Interact.*, **15**, doi:10.1175/2010EI363.1.

Mitchell, K.E., and Coauthors, 2004: The multi-institution North American Land Data Assimilation System (NLDAS): Utilizing multiple GCIP products and partners in a continental distributed hydrological modeling system, *J. Geophys. Res.*, **109**, D07S90, doi:10.1029/2003JD003823.

Mo, K.C., and D.P. Lettenmaier, 2015: Heat wave flash droughts in decline. *Geophys. Res. Lett.*, **42**, 2823–2829, doi:10.1002/2015GL064018.

Monteith, J.L., 1965: Evaporation and environment. *Symp. Soc. Exp. Biol.*, **XIX**, 205–234.

Mu, Q., M. Zhao, J.S. Kimball, N.G. McDowell, and S.W. Running, 2013: A remotely sensed global terrestrial drought severity index. *Bull. Amer. Meteor. Soc.*, **94(1)**, 83–98, doi:10.1175/BAMS-D-11-00213.1.

Otkin, J.A., M.C. Anderson, C. Hain, I.E. Mladenova, J.B. Basara, M. Svoboda, 2013a: Examining rapid onset drought development using the thermal infrared–based Evaporative Stress Index. *J. Hydrometeor.*, **14**, 1057–1074. doi:10.1175/JHM-D-12-0144.1.

Otkin, J.A., M.C. Anderson, C. Hain, and M. Svoboda, 2013b: Examining the relationship between drought development and rapid changes in the Evaporative Stress Index. *J. Hydrometeor.*, **15**, 938–956, doi:10.1175/JHM-D-13-0110.1.

Palmer, W.C., 1965: Meteorological drought. Research Paper 45, 58 pp. [Available online at http://www.ncdc.noaa.gov/temp-and-precip/drought/docs/palmer.pdf.]

Penman, H.L., 1948: Natural evaporation from open water, bare soil and grass. *Proc. R. Soc. London, Ser. A*, **193(1032)**, 120–146, doi:10.1098/rspa.1948.0037.

Priestley, C.H.B., and R.J. Taylor, 1972: On the assessment of surface heat flux and evaporation using large-scale parameters. *Mon. Weather Rev*., **100(2)**, 81–92.

Quiring, S.M., 2009: Developing objective operational definitions for monitoring drought. *J. Appl. Meteor. Climatol.* **48**, 1217–1229, doi: 10.1175/2009JAMC2088.1.

Ralph, F.M., and M.D. Dettinger, 2012: Historical and national perspectives on extreme West Coast precipitation associated with atmospheric rivers during December 2010. *Bull. Amer. Meteor. Soc.*, **93**, 783–790. doi:10.1175/BAMS-D-11-00188.1.

Seager, R., 2007: The turn of the century North American drought: global context, dynamics, and past analogs. *J. Climate*, **20**, 5527–5552, doi:10.1175/2007JCLI1529.1.

Seager, R., M. Hoerling, S. Schubert, H. Wang, B. Lyon, A. Kumar, J. Nakamura, and N. Henderson, 2014: Causes and predictability of the 2011-14 California drought. Assessment Report, 40 pp. [Available online at http://cpo.noaa.gov/MAPP/californiadroughtreport.]

Sheffield, J., E.F. Wood, and M.L. Roderick, 2012: Little change in global drought over the past 60 years. *Nature*, **491**, 435–438, 15 November, doi:10.1038/nature11575.

Svoboda, M., and Coauthors, 2002: The Drought Monitor. *Bull. Amer. Meteor. Soc*., **83**, 1181–1190.

Thornthwaite, C.W., 1948: An approach toward a rational classification of climate. *Geogr. Rev.*, **38**, 55–94.

Trouet, V., A.H. Taylor, A.M. Carleton, and C.N. Skinner, 2009: Interannual variations in fire weather, fire extent, and synoptic-scale circulation patterns in northern California and Oregon. *Theor. Appl. Climatol.*, **95(3-4)**, 349–360, doi:10.1007/s00704-008-0012-x.

van der Schrier, G., P.D. Jones, and K.R. Briffa, 2011: The sensitivity of the PDSI to the Thornthwaite and Penman-Monteith parameterizations for potential evapotranspiration. *J. Geophys. Res.*, **116**, doi:10.1029/2010JD015001.

Vicente-Serrano, S.M., J.I. López-Moreno, S. Beguería, J. Lorenzo-Lacruz, C. Azorin-Molina, and E. Morán-Tejeda, 2012: Accurate computation of a streamflow drought index. *J. Hydrol. Eng.*, **17(2)**, 318–332, doi:10.1061/(ASCE)HE.1943-5584.0000433.

Weiss, J.L., C.L. Castro, and J.T. Overpeck, 2009: Distinguishing pronounced droughts in the southwestern United States: Seasonality and effects of warmer temperatures. *J. Climate*, **22**, 5918–5932, doi: 10.1175/2009JCLI2905.1.

Wilks, D.S., 2011: Empirical distributions and exploratory data analysis. *Statistical methods in the atmospheric sciences.* Academic Press, 23–70.

Xia, Y. and Coauthors, 2012a: Continental-scale water and energy flux analysis and validation for the North American Land Data Assimilation System project phase 2 (NLDAS-2): 1. Intercomparison and application of model products. *J. Geophys. Res.*, **117(D3)**, doi:10.1029/2011JD016048.

Xia, Y. and Coauthors, 2012b: Continental-scale water and energy flux analysis and validation for the North American Land Data Assimilation System project phase 2 (NLDAS-2): 2. Validation of model-simulated streamflow, *J. Geophys. Res.*, **117(D3)**, doi:10.1029/2011JD016051.

Yao, Y., S. Liang, Q. Qin, and K. Wang, 2010: Monitoring drought over the conterminous United States using MODIS and NCEP Reanalysis-2 data. *J. Appl. Meteor. Climatol*., **49**, 1665–1680. doi:10.1175/2010JAMC2328.1.

Table 1: Drought classes for comparing USDM to SPI, SSI, ESI, and EDDI. Positive EDDI values indicate drought and the upper percentiles (70-100) must be used to derive USDM classes.

USDM drought category	Description	SPI, SSI, and ESI percentiles	EDDI percentiles
D0	Abnormally Dry	21-30	70-79
D1	Moderate Drought	11-20	80-89
D2	Severe Drought	6-10	90-94
D3	Extreme Drought	3-5	95-97
D4	Exceptional Drought	0-2	98-100

List of figures:

Figure 1: Correlation coefficient between EDDI and SPI at **(a)** 1-month, **(c)** 6-month, **(e)** 12-month, and SSI **(b)** 1-month, **(d)** 6-month, and **(f)** 12-month time scales.

Figure 2: Shading indicates METDATA terrain height (m) and red boxes indicate area-averaging domains for Figures 3 and 4. IA, TX, and PA boxes are 50 x 100 4-km METDATA pixels (200 km x 400 km), and CA box is 25 x 25 pixels (100 km x 100 km).

Figure 3: Monthly correlations between EDDI and SPI (top row) and SSI (bottom row) at all time scales for **(a, e)** TX, **(b, f)** CA, **(c, g)** IA, and **(d, h)** PA. Y-axis indicates ending month of each time scale, and x-axis shows time scale (months). Shading indicates correlation coefficients.

Figure 4: Lagged correlation between 3-month SSI ending in August and EDDI for **(a)** CA, **(b)** TX, **(c)** IA, and **(d)** PA. Y-axis indicates EDDI ending months and x-axis indicate EDDI time scale. Green dots are placed in the ending month containing the strongest correlation for each time scale, and blue dots are used as a reference to show SSI time scale and ending month.

Figure 5: Seasonal correlation coefficient (left column spring and right column summer) between ESI and EDDI at **(a, b)** 4-week, **(c, d)** 8-week, and **(e, f)** 12-week time scales. Areas shaded in white indicate an insufficient amount of ESI data.

Figure 6: EDDI under sustained and flash drought conditions. **(a)** Monthly time series of 1-month EDDI, SSI, and SPI area averaged over the IA domain. **(b)** Monthly time series of 1-month EDDI and EDDI constrained by climatology T_{air} (EDDI-T), q (EDDI-q), R_d (EDDI-R_d), and U_2 (EDDI- U_2). Black box highlights time period shown in (c). **(c)** Daily time series of 1-month EDDI, EDDI-T, EDDI-q, EDDI-R_d and EDDI-U_2 for May and June 2011 shown to highlight details of flash drought initiation. Note that the vertical axis of EDDI is reversed

to clearly visualize drought onset and duration when compared to SPI and SSI. Light green reference line indicates start of moderate drought classification (-0.78).

Figure 7: Evolution of the 1-month EDDI **(top row)**, USDM **(second row)**, 1-month ESI **(third row)**, 1-month SSI **(fourth row)**, and 1-month SPI **(fifth row)** through spring and summer of 2012. USDM data are from 1 May, 2012 (April column), 5 June, 2012 (May column), 3 July, 2012 (June column), and 31 July, 2012 (July column). EDDI, ESI, SSI, and SPI are at 1-month time scales at the end of each month: April, May, June, and July. All drought metrics have been converted to USDM categories according to **Table 1**.

Figure 8: USDM from 02 October, 2007 **(a)** and 25 June, 2002 **(b)**, 12-month (October-September) EDDI **(c)**, SSI **(e)**, and SPI **(g)** ending September, 2007, and 6-month (January-June) EDDI **(d)**, SSI **(f)**, and SPI **(h)** ending June, 2002.

Figure 9: Area-averaged time series of EDDI over the northern Sierra Nevada from 1979 to 2013 aggregated at 2-week (a), 1-month (b), 3-month (c), 6-month (d), and 12-month time scales.

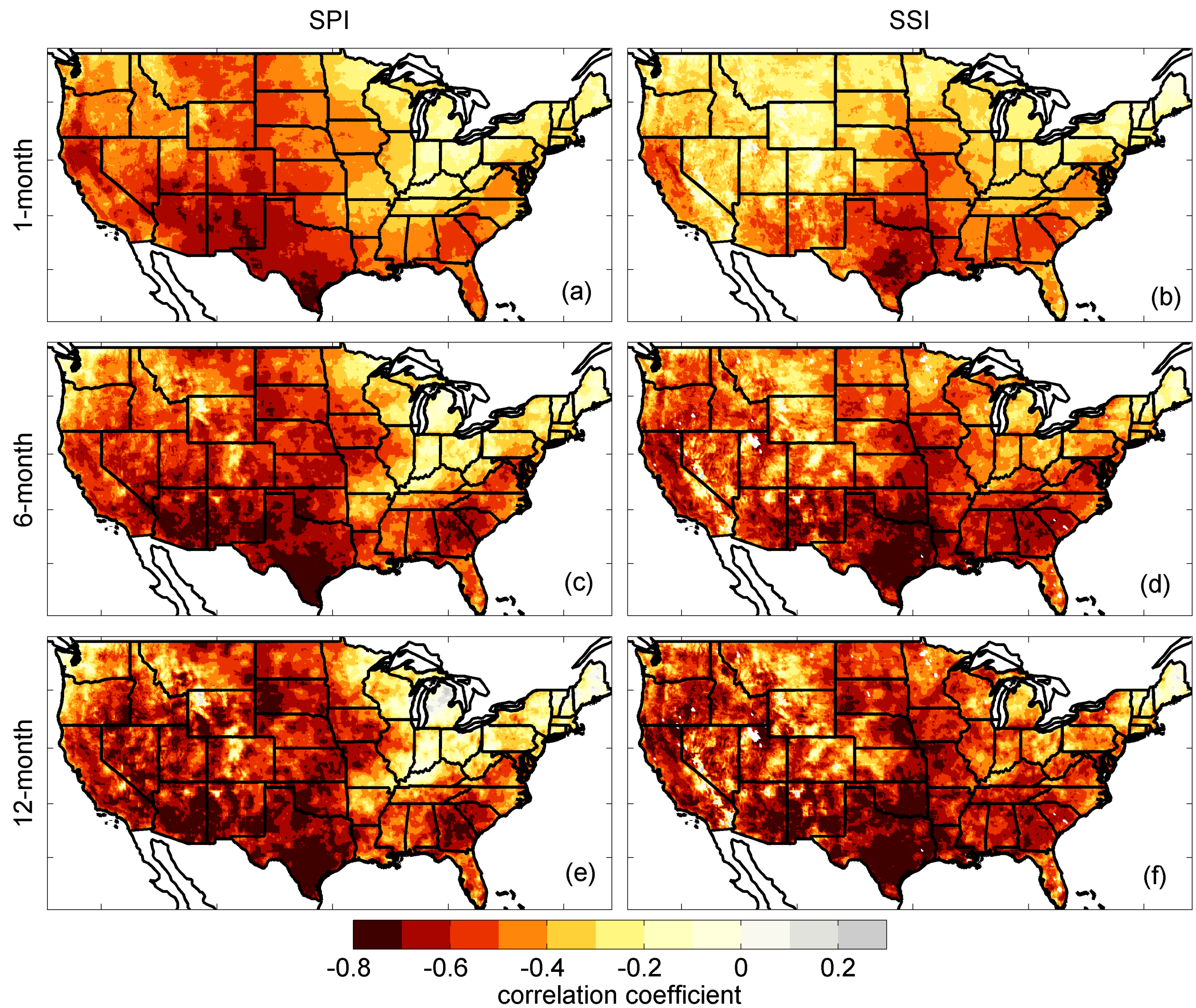

Figure 1: Correlation coefficient between EDDI and SPI at **(a)** 1-month, **(c)** 6-month, **(e)** 12-month, and SSI **(b)** 1-month, **(d)** 6-month, and **(f)** 12-month time scales.

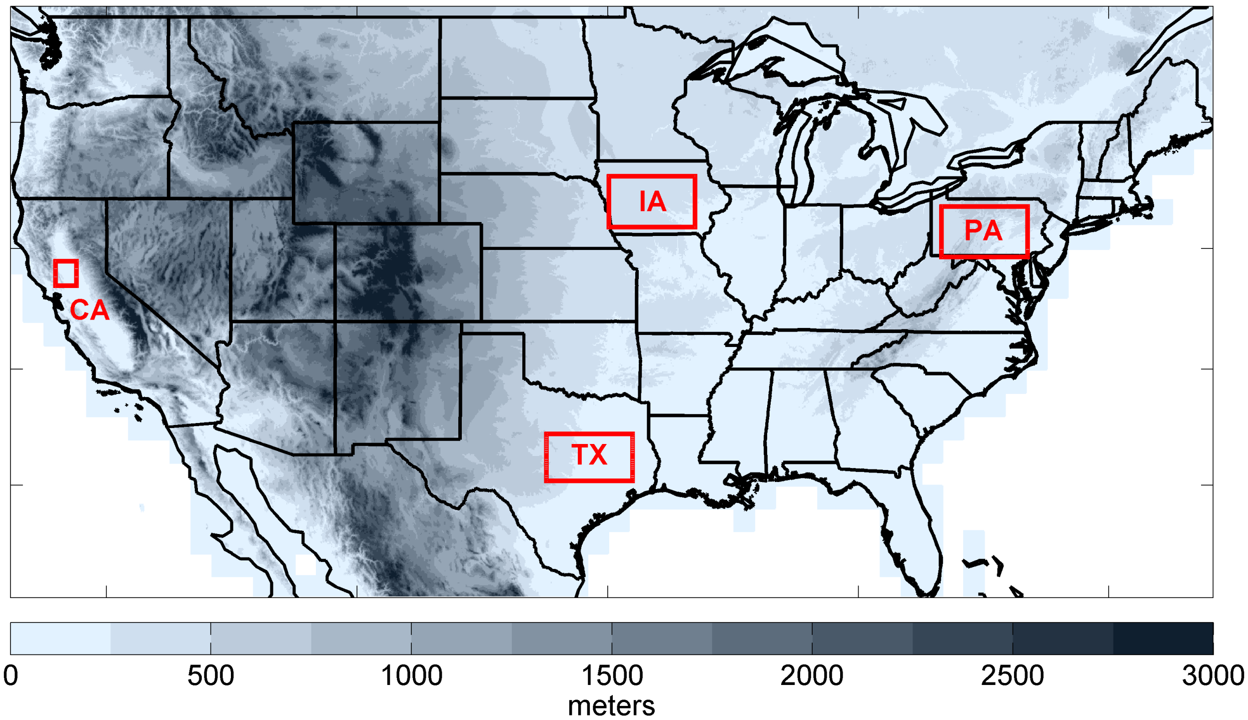

Figure 2: Shading indicates METDATA terrain height (m) and red boxes indicate area-averaging domains for Figures 3 and 4. IA, TX, and PA boxes are 50 x 100 4-km METDATA pixels (200 km x 400 km), and CA box is 25 x 25 pixels (100 km x 100 km).

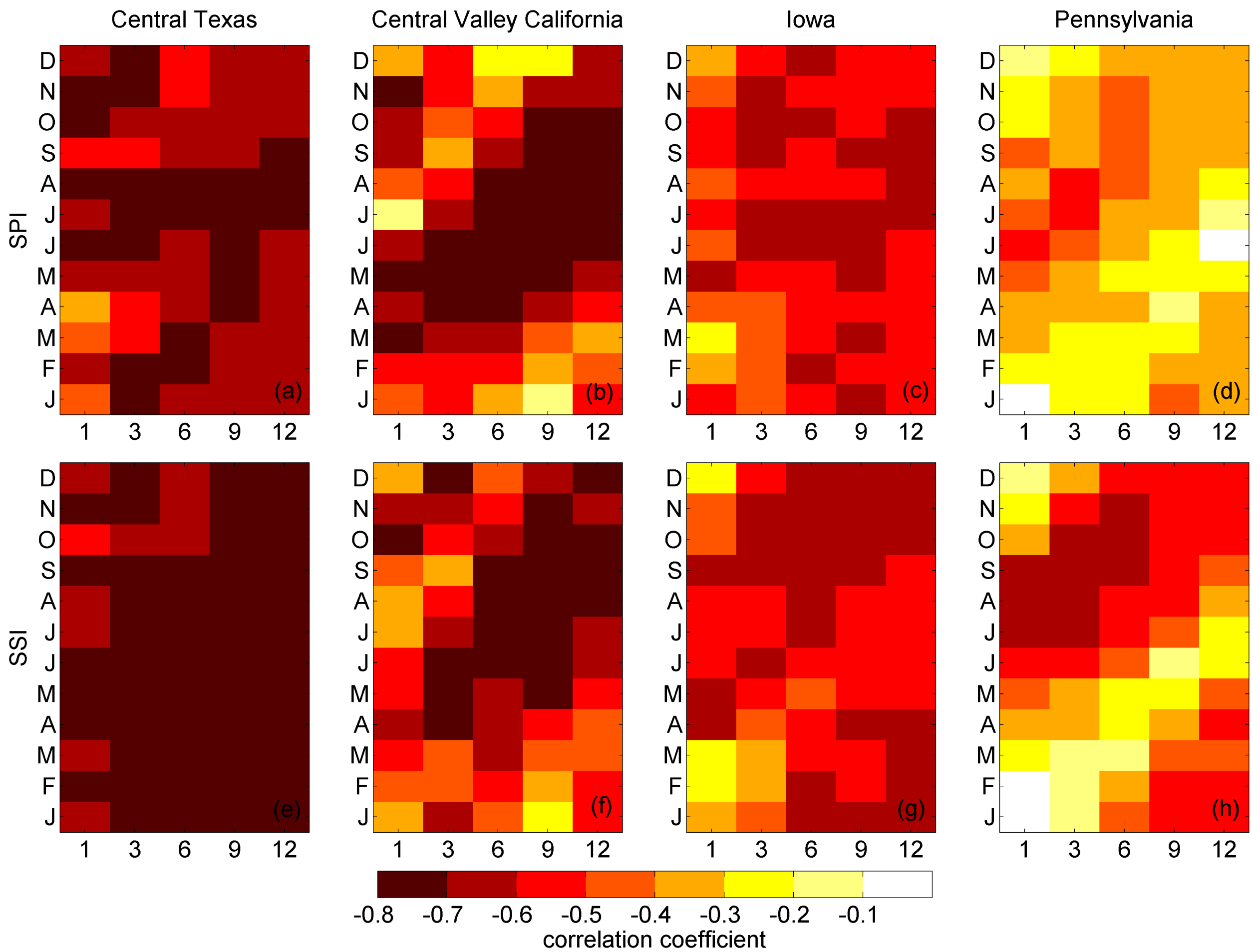

Figure 3: Monthly correlations between EDDI and SPI (top row) and SSI (bottom row) at all time scales for **(a, e)** TX, **(b, f)** CA, **(c, g)** IA, and **(d, h)** PA. Y-axis indicates ending month of each time scale, and x-axis shows time scale (months). Shading indicates correlation coefficients.

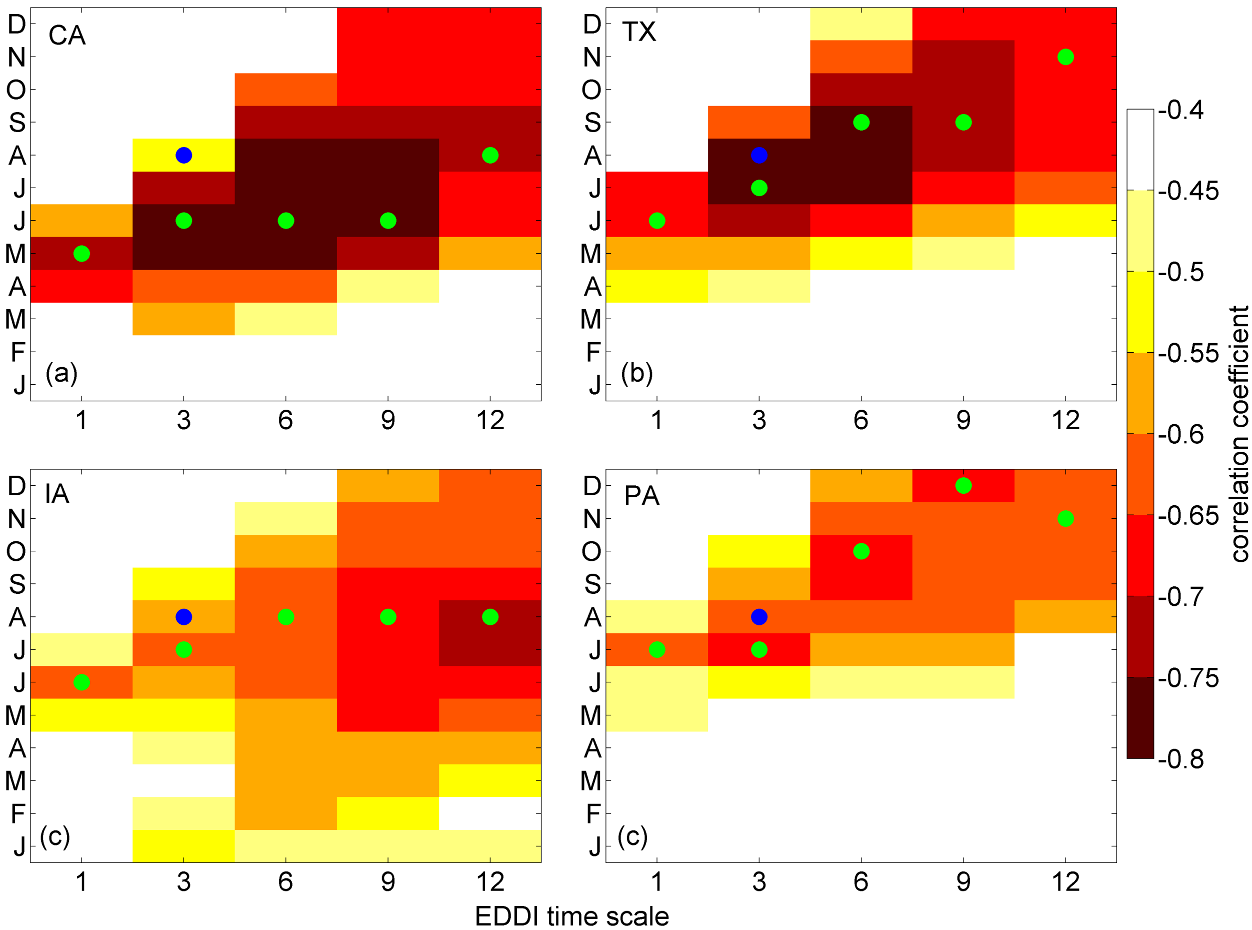

Figure 4: Lagged correlation between 3-month SSI ending in August and EDDI for **(a)** CA, **(b)** TX, **(c)** IA, and **(d)** PA. Y-axis indicates EDDI ending months and x-axis indicate EDDI time scale. Green dots are placed in the ending month containing the strongest correlation for each time scale, and blue dots are used as a reference to show SSI time scale and ending month.

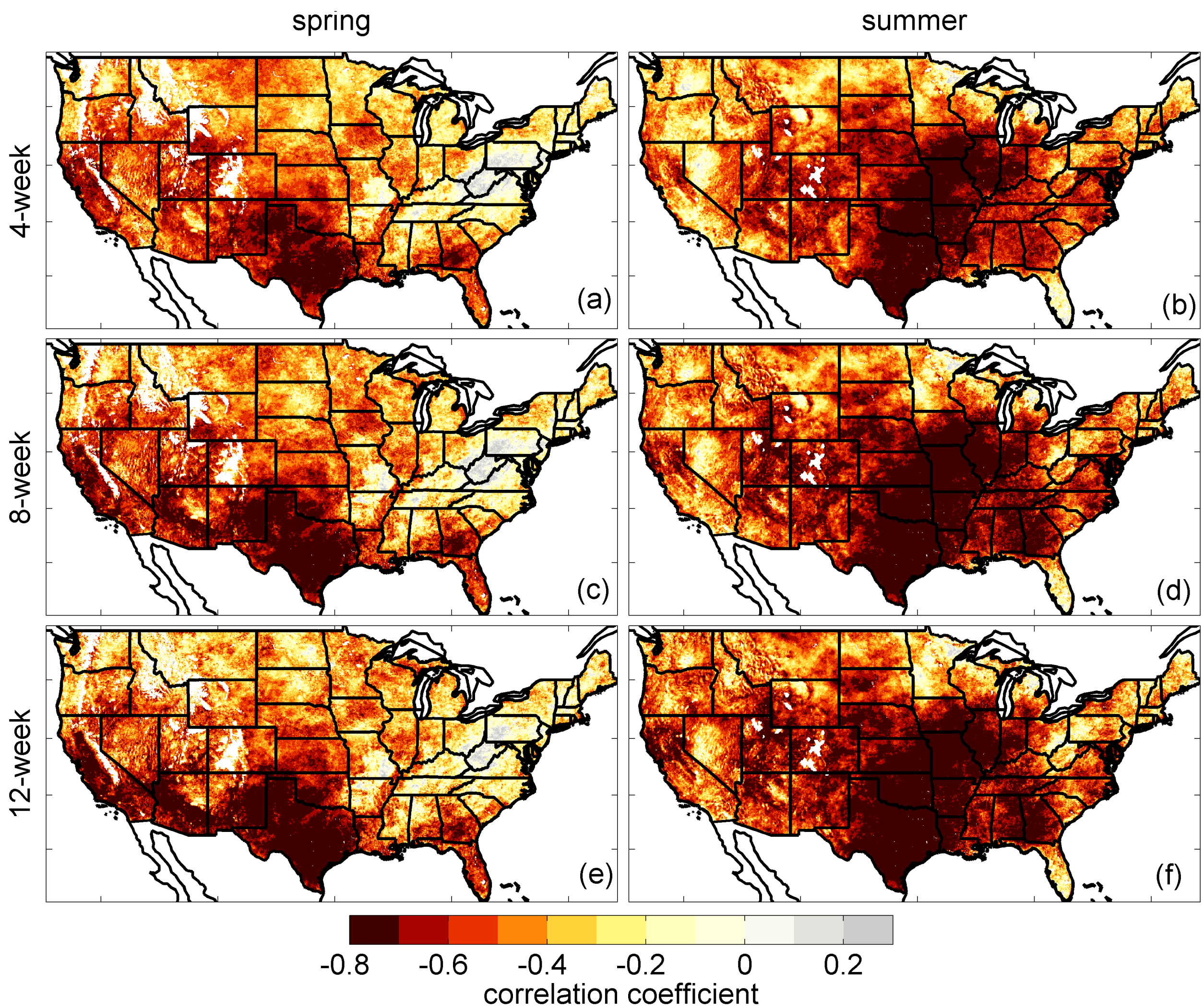

Figure 5: Seasonal correlation coefficient (left column spring and right column summer) between ESI and EDDI at **(a, b)** 4-week, **(c, d)** 8-week, and **(e, f)** 12-week time scales. Areas shaded in white indicate an insufficient amount of ESI data.

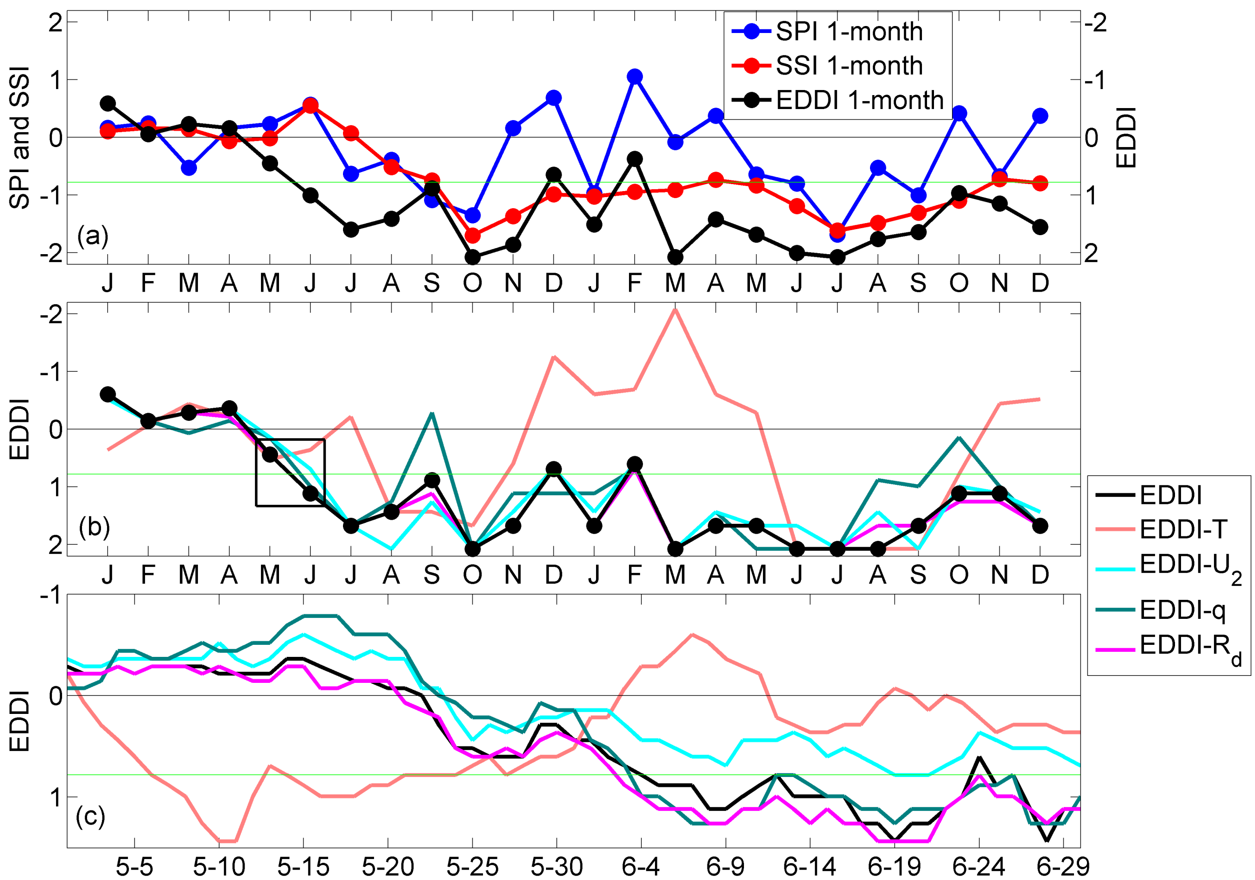

Figure 6: EDDI under sustained and flash drought conditions. **(a)** Monthly time series of 1-month EDDI, SSI, and SPI area averaged over the IA domain. **(b)** Monthly time series of 1-month EDDI and EDDI constrained by climatology T_{air} (EDDI-T), *q* (EDDI-q), R_d (EDDI-R_d), and U_2 (EDDI- U_2). Black box highlights time period shown in (c). **(c)** Daily time series of 1-month EDDI, EDDI-T, EDDI-q, EDDI-R_d and EDDI-U_2 for May and June 2011 shown to highlight details of flash drought initiation. Note that the vertical axis of EDDI is reversed to clearly visualize drought onset and duration when compared to SPI and SSI. Light green reference line indicates start of moderate drought classification (-0.78).

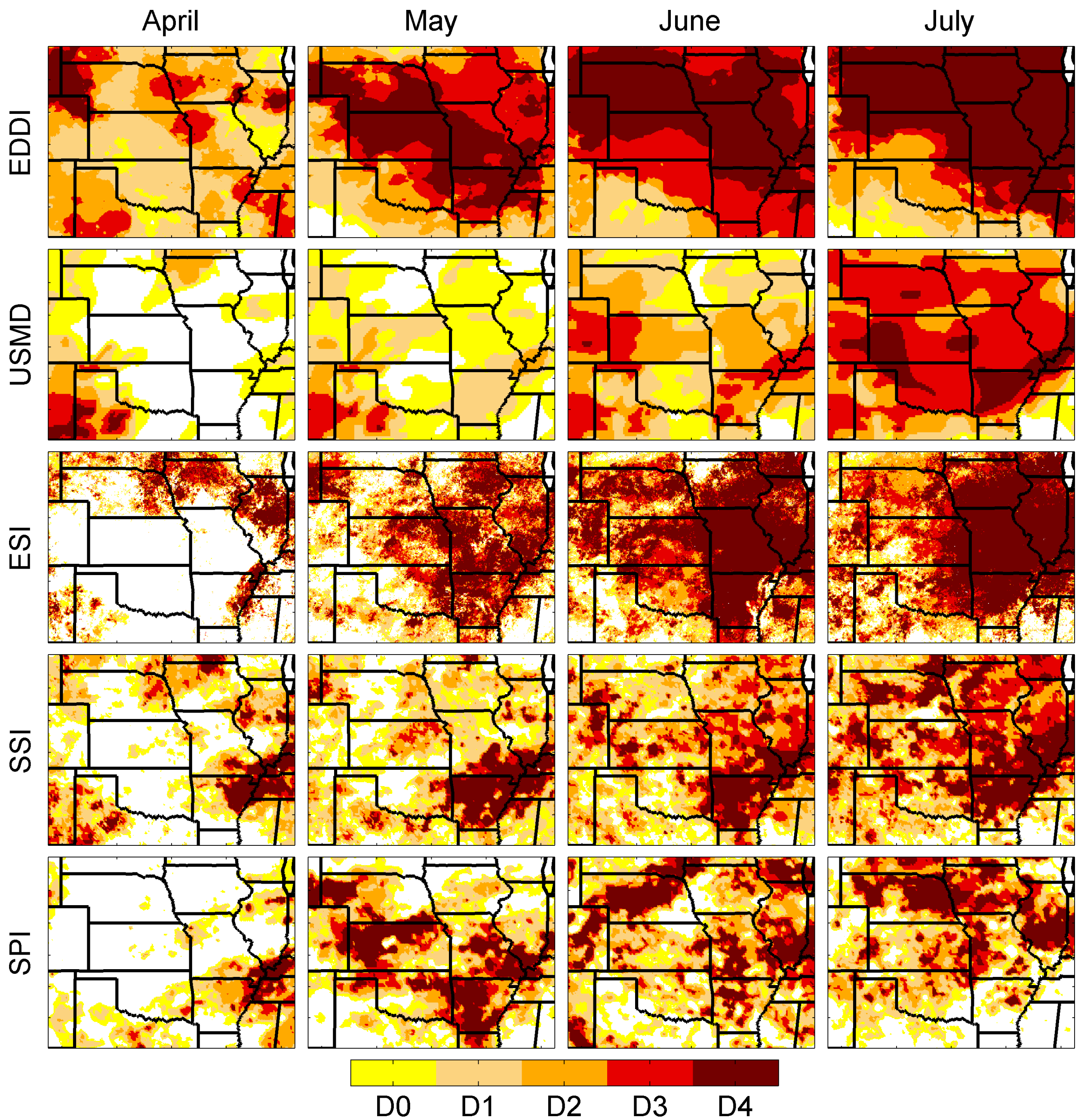

Figure 7: Evolution of the 1-month EDDI **(top row)**, USDM **(second row)**, 1-month ESI **(third row)**, 1-month SSI **(fourth row)**, and 1-month SPI **(fifth row)** through spring and summer of 2012. USDM data are from 1 May, 2012 (April column), 5 June, 2012 (May column), 3 July, 2012 (June column), and 31 July, 2012 (July column). EDDI, ESI, SSI, and SPI are at 1-month time scales at the end of each month: April, May, June, and July. All drought metrics have been converted to USDM categories according to **Table 1**.

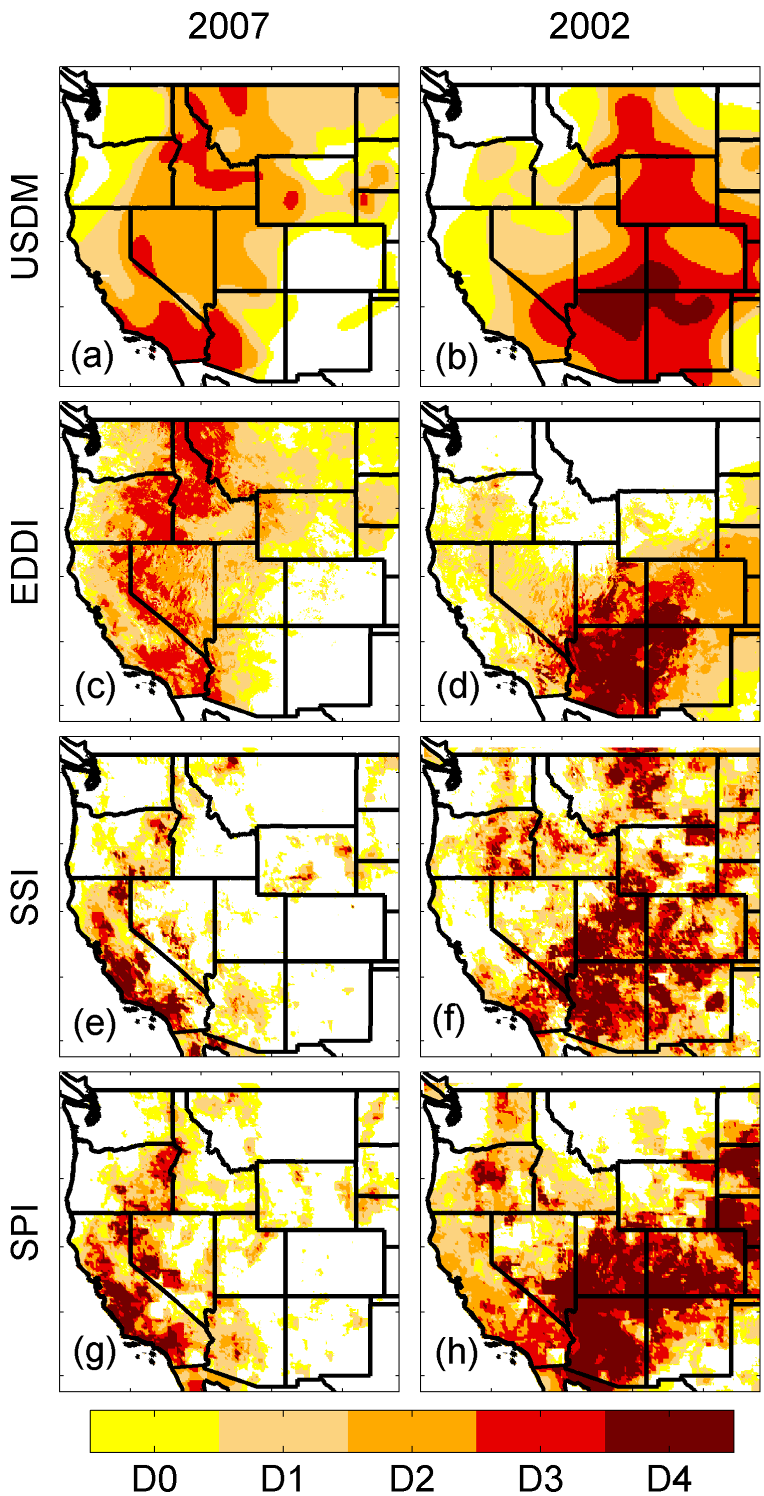

Figure 8: USDM from 02 October, 2007 **(a)** and 25 June, 2002 **(b)**, 12-month (October-September) EDDI **(c)**, SSI **(e)**, and SPI **(g)** ending September, 2007, and 6-month (January-June) EDDI **(d)**, SSI **(f)**, and SPI **(h)** ending June, 2002.

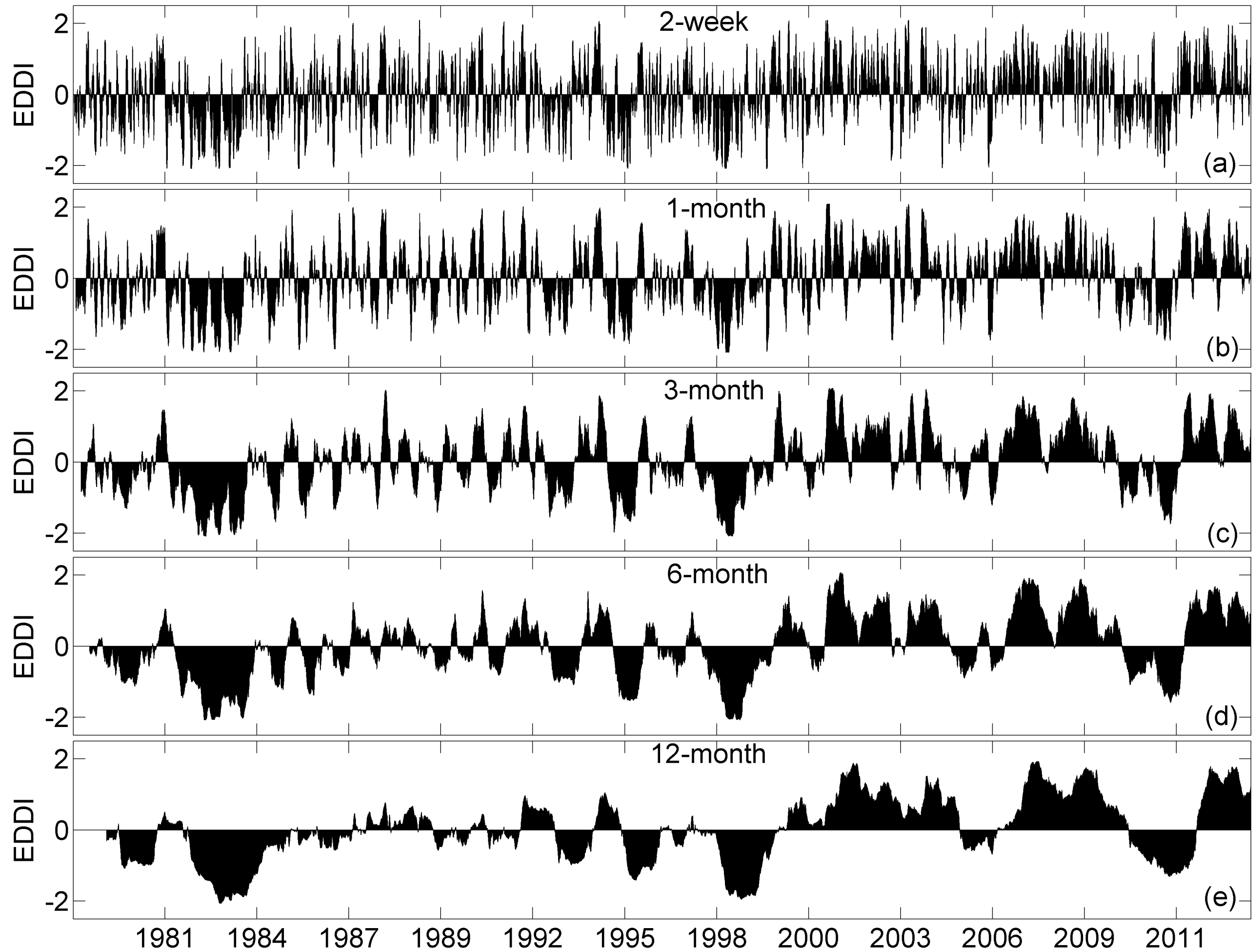

Figure 9: Area-averaged time series of EDDI over the northern Sierra Nevada from 1979 to 2013 aggregated at 2-week (a), 1-month (b), 3-month (c), 6-month (d), and 12-month time scales.